UCRL-PROC-218581

LAWRENCE
LIVERMORE
NATIONAL
LABORATORY

Influence of Hydrologic Heterogeneity on Thermal-Hydrologic Behavior in Emplacement Drifts

Y. Sun, T. A. Buscheck, Y. Hao

February 1, 2006

International High-Level Radioactive Waste Management Conference
Las Vegas, NV, United States
April 30, 2006 through May 4, 2006

This document was prepared as an account of work sponsored by an agency of the United States Government. Neither the United States Government nor the University of California nor any of their employees, makes any warranty, express or implied, or assumes any legal liability or responsibility for the accuracy, completeness, or usefulness of any information, apparatus, product, or process disclosed, or represents that its use would not infringe privately owned rights. Reference herein to any specific commercial product, process, or service by trade name, trademark, manufacturer, or otherwise, does not necessarily constitute or imply its endorsement, recommendation, or favoring by the United States Government or the University of California. The views and opinions of authors expressed herein do not necessarily state or reflect those of the United States Government or the University of California, and shall not be used for advertising or product endorsement purposes.

Updated October 14, 2003

Influence of Hydrologic Heterogeneity on Thermal-Hydrologic Behavior in Emplacement Drifts

Yunwei Sun, Thomas A. Buscheck, and Yue Hao
L-631, Lawrence Livermore National Laboratory, Livermore, CA 94551

Abstract – *Fracture networks have been characterized as highly permeable continuum within the porous rock matrix in thermal-hydrologic models used to support performance assessments of the proposed nuclear-waste repository at Yucca Mountain. Uncertainty and spatial variability of the fracture permeability are important considerations for understanding thermal-hydrologic behavior within the host rock surrounding an emplacement drift. In this paper, we conducted numerical experiments with a number of realizations of intrinsic fracture permeability and examine thermal conditions around an emplacement drift. Peak temperature and boiling duration on the drift wall are used as indices to quantify the influence of fracture permeability. The variability of peak temperature and boiling duration resulting from small-scale fracture-permeability heterogeneity is compared with the variability resulting from variability of host-rock thermal conductivity and infiltration flux. An examination of rock dryout and condensate drainage shows that small-scale heterogeneity in fracture permeability results in a relatively small range in dryout volume and does not prevent the shedding of condensate through the pillar-separating emplacement drifts.*

I. INTRODUCTION

Hydrogeologic-property heterogeneity and its effect on flow and transport processes has been extensively studied in the past using a variety of analytical and numerical methods [1, 2]. Characterization of hydrologic heterogeneity has been an important issue in Yucca Mountain Project [3, 4, 5]. The influence of spatial variability of hydrologic parameters (such as intrinsic fracture permeability, porosity, and matrix capillary parameters) on seepage into emplacement drifts has received considerable attention [6, 7, 8]. Sensitivity analysis of thermal properties has been conducted by Glascoe et al. [11]. The objective of this study is to investigate the influence of fracture-permeability heterogeneity, within the host rock surrounding an emplacement drift, on near-field and in-drift thermal-hydrologic (TH) behavior. The emphasis is temperature, which is a key TH variables, predicted by the MultiScale Thermohydrologic Model (MSTHM) [9, 10], and required by downstream process models supporting the performance assessment of the proposed nuclear-waste repository at Yucca Mountain. Using TH submodels from the family of MSTHM models, magnitudes of each quantified impact are assessed and compared with the influence of parametric uncertainty that has been addressed in MSTHM-predicted TH conditions within drifts [9, 10], which have been used in the performance assessment of the proposed Yucca Mountain repository.

II. MODEL DESCRIPTION

Our model solves the balance equations of air, water, and energy components for liquid and gas phases in a nondeformable dual-porosity domain [12]. The mass balance equations for the air and water components are

$$\frac{\partial}{\partial t}\left(\sum_{\alpha}\phi\rho_{\alpha}S_{\alpha}\omega_{\alpha}^{\gamma}\right)=-\sum_{\alpha}\nabla\cdot\phi\rho_{\alpha}S_{\alpha}\left(\omega_{\alpha}^{\gamma}\mathbf{v}_{\alpha}+\mathbf{J}_{\alpha}^{\gamma}\right) \qquad (1)$$

where

t	is time,
γ	is a component (air or water),
α	is a fluid phases (liquid or gas),
ω_{α}^{γ}	is mass fraction of γ component in phase α,
ϕ	is porosity,
ρ_{α}	is density of α phase,
S_{α}	is saturation of α phase,
$\mathbf{v}_{\alpha}$	is vector of velocity,
J_{α}^{γ}	is combined diffusive and dispersive flux.

Mass-transport mechanisms include advection and diffusion/dispersion for two components (air and water) in two phases (liquid and gas). The combined diffusive and dispersive fluxes are described by Fick's law and the advective flux is described by Darcy's law,

$$\mathbf{J}_{\alpha}^{\gamma}=-\nabla\cdot\left(\mathbf{D}_{\alpha}^{\gamma}\ \omega_{\alpha}^{\gamma}\right) \qquad (2)$$

$$S_{\alpha}\phi\mathbf{v}_{\alpha}=-\frac{\kappa_{\alpha}(S_{\alpha})}{\mu_{\alpha}}\left(\nabla p_{\alpha}+\rho_{\alpha}g\nabla z\right) \qquad (3)$$

where $\mathbf{D}_{\alpha}^{\gamma}$ is a tensor of the combined diffusion and dispersion coefficients, k_{α} is permeability function, is viscosity of α phase, p_{α} is α phase pressure, and g is gravitational acceleration.

Heat-transport mechanisms include advection and diffusion/dispersion (in terms of mass flux) for two phases, thermal conduction in three phases (including solid phase), and radiative heat transfer for elements representing the open repository drift in which the waste package, drip shield, and invert are implemented (Fig. 1).

The energy balance equation is

$$\frac{\partial}{\partial t}\left[\sum_{\alpha}\phi\rho_{\alpha}u_{a}S_{\alpha}+(1-\phi)\rho_{s}C_{p}(T-T_{ref})\right]= -\sum_{\gamma}\sum_{\alpha}\left[\nabla\cdot\phi h_{\alpha}^{\gamma}\rho_{\alpha}S_{\alpha}\left(\omega_{\alpha}^{\gamma}\mathbf{v}_{\alpha}+\mathbf{J}_{\alpha}^{\gamma}\right)\right] +\nabla\cdot K\nabla T \qquad (4)$$

where

T	is temperature,
T_{ref}	is reference temperature,
C_p	is specific heat of solid,
ρ_s	is density of solid phase,
u_α	is specific internal energy,
ρ_α	is density of α phase,
h_α^γ	is partial specific enthalpy of γ in α,
K	is thermal conductivity.

Our model utilizes a dual-permeability approach to treat fractures and rock matrix as two separate continua with a complete set of mass and energy balance equations and computational grids for each continuum. A linear function is used to describe the exchange terms for mass and energy between the two continua. The relationships between permeability, saturation, and capillary pressures described by the formulations of van Genuchten [13] are modified to account for the active fracture concept [14].

For a location close to the center of the repository, a 2-D Line-averaged-heat-source, Drift-scale Thermal-Hydrologic (LDTH) submodel is selected from the family of MSTHM submodels [9, 10] to be applied as the base model used in this study. A log-normal distribution of a random field is used to represent drift-scale heterogeneity of fracture permeability of the host rock:

$$p(\mathbf{x})\approx\mu(\mathbf{x})+p'\left[\sigma,\varepsilon(\mathbf{x})\right] \qquad (5)$$

where $p(\mathbf{x})$ is the random field of *log k*; p' is the perturbation of $p(\mathbf{x})$, which is a function of standard deviation σ and the normalized perturbation $\varepsilon(\mathbf{x})$ of zero-mean and unity standard deviation; and $\mu(\mathbf{x})$ is the mean of *log k.* Since only one host-rock material type (or unit) is considered, μ is independent of spatial coordinates.

To investigate the impact of small-scale (1-m × 2-m scale) heterogeneity in fracture permeability on dryout and condensate shedding around emplacement drifts, the LDTH submodel [9, 10] is modified to have a fine numerical mesh around the emplacement drift, with maximum dimensions of 2-m high by 1-m wide, for the entire lateral extent of the submodel (40.5 m), which is the half-distance between emplacement drifts, and vertically extending from 37.75 m above the emplacement drift, to 37.75 m below the drift. Random fracture permeability fields are generated for a regular 1-m high by 1-m wide grid and remapped onto the LDTH-submodel mesh. These heterogeneous fields conserve the fracture permeability over this 81-m by 40.5-m domain, which is entirely within the Tptpll (tsw35) unit for the homogeneous case [9, 10]. The LDTH-submodel calculations were conducted for 20,100 years, for two groups of 100 realizations each. The stochastic fields for the two families of 100 realizations are generated on the basis of the respective log-normal distributions. These distributions are developed for a standard deviation σ of 1 and 2, respectively. These stochastic fields apply a correlation factor of 0.2, which is equivalent to a correlation length of approximately 4 m. The exponential covariance function is used to generate covariance matrix.

Peak temperatures and boiling duration are examined on the drift wall, above the dripshield, and above the spring line, as shown in Fig. 1. Results from infiltration-flux and host-rock thermal-conductivity uncertainty studies [9, 10] are used as references to compare against the influence of fracture permeability on the peak temperatures and boiling duration (Table I).

TABLE I. Case definitions.

Case	Definition		
	Infiltration	Thermal Conductivity	Fracture Permeability
LI-lkt	Lower bound	Low	Mean
MI-mkt	Mean	Mean	Mean
UI-hkt	Upper bound	High	Mean
Case 1	Mean	Mean	$\sigma = 1.0$
Case 2	Mean	Mean	$\sigma = 2.0$

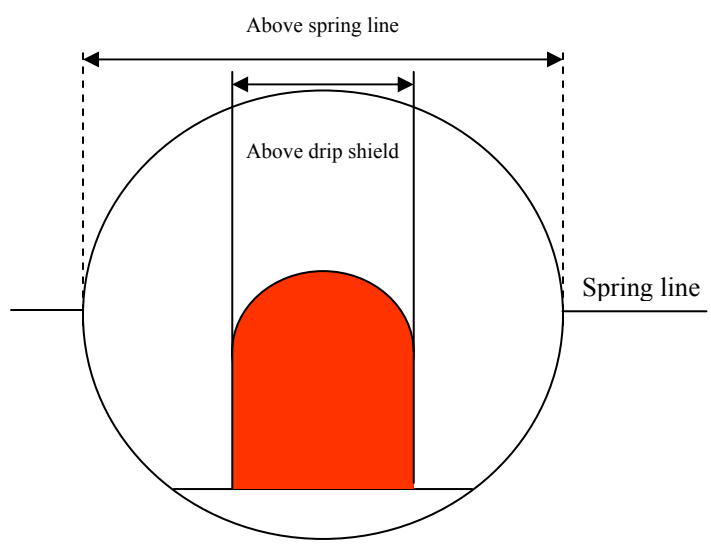

Fig. 1. Graphic definition of entire drift wall, above the drip shield, and above the spring line.

III. MODEL RESULTS

The focus factor is defined as the local vertical percolation flux divided by the average percolation flux (4.71 mm/yr), which is a typical value for the modern climate at the repository location selected for this study [9, 10]. Thus, a local focus factor of 5 corresponds to a local percolation flux of 23.55 mm/yr for this example. The range in focus factor (from the minimum to the maximum value) is given for 100 realizations with $\sigma = 1.0$ (Fig. 2a) and for 100 realizations for $\sigma = 2.0$ (Fig. 2b). As evident in Fig. 2, the minimum focus factor is nearly 0.0 for all lateral distances from the drift centerline, while the maximum focus factor varies by about a factor of two. Averaged over the interval between the drift and pillar centerlines, the maximum focus factor is 3.407 for the 100 realizations with $\sigma = 1.0$ and is 5.139 for the 100 realizations with $\sigma = 2.0$. The small variability in the minimum and maximum focus factor indicates that 100 realizations are sufficient to capture the influence of small-scale heterogeneity on flow focusing.

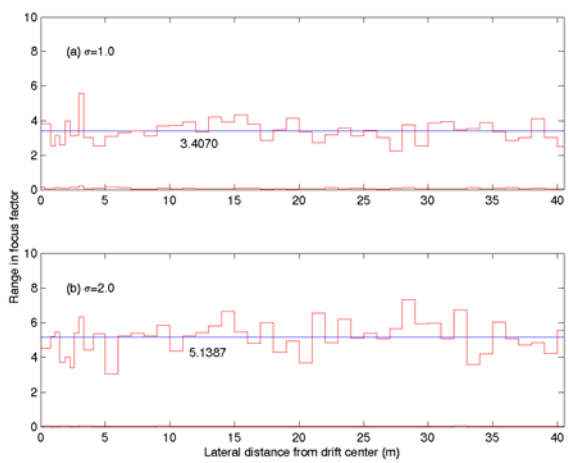

Fig. 2. Range in focus factor versus lateral distance from the drift centerline for (a) 100 realizations with $\sigma = 1.0$ and (b) 100 realizations with $\sigma = 2.0$

The approach used in this study to determine the focus factor is similar to that used elsewhere [7], both with respect to the conceptual model [14], the spatial resolution of the numerical models (e.g., see [7], Figs.6.6-13 and 6.6-14), and the results of the respective studies. Fig. 3 shows lateral distribution of the focus factor from the drift centerline to the pillar centerline at an elevation immediately above the crown of the drift or these four end-member realizations with respect to thermal-hydrologic behavior. Realizations R82 and R100 have a large focus factor immediately above the drift, which enhances rewetting of the dryout zone, thereby reducing the magnitude and duration of temperature buildup around the drift. Realizations R64 and R09 have small focus factors immediately above the drift, which allows the development of a larger and more persistent dryout zone, thereby increasing the magnitude and duration of temperature buildup around the drift.

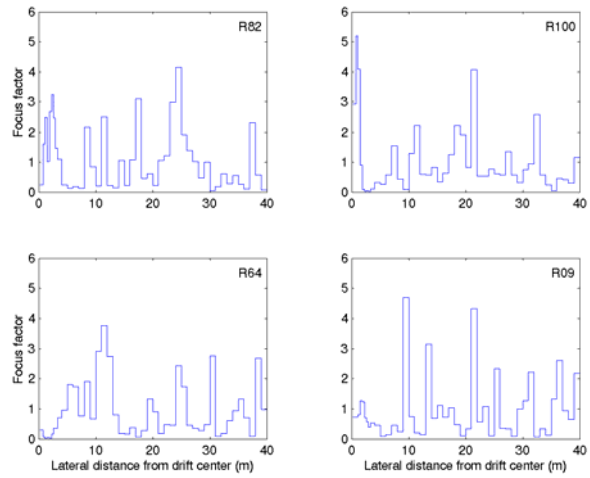

NOTE: The focus factor is defined to be the local vertical percolation flux divided by the average percolation flux, which is 4.71 mm/yr at this location. These four realizations result in end-member thermal-hydrologic behavior for the respective 100 realizations, with realizations R82 and R100 resulting in relatively short boiling durations on the drift wall and realizations R64 and R09 resulting in relatively long boiling durations on the drift wall.

Fig. 3. Lateral distribution of the focus factor at an elevation immediately above the crown of the drift for four realizations when $\sigma = 2.0$

Figs. 4, 5, and Table II show the sensitivity of peak drift-wall temperature to small-scale heterogeneity in fracture permeability. For 100 realizations with $\sigma = 1.0$ and 100 realizations with $\sigma = 2.0$, the mean temperature history is nearly the same as the temperature history for the corresponding homogeneous case. The mean peak drift-wall temperature is virtually the same for the 100 realizations with $\sigma = 1.0$ and with $\sigma = 2.0$, which are virtually the same as the peak drift-wall temperature for the homogeneous case [9, 10]. The minimum peak drift-wall temperature is nearly the same for $\sigma = 1.0$ and 2.0, while the maximum peak drift-wall temperature is nearly the same for $\sigma = 1.0$ and 2.0. The range in peak drift-wall temperature is 7.8 and 8.0^{o}C for $\sigma = 1.0$ and 2.0, respectively, while the range in peak drift-wall temperature arising from parametric uncertainty is 44.5^{o}C. Thus, the influence of small-scale heterogeneity in fracture permeability on peak drift-wall temperature is insignificant compared to that of parametric uncertainty, which has been addressed in the MSTHM [9, 10].

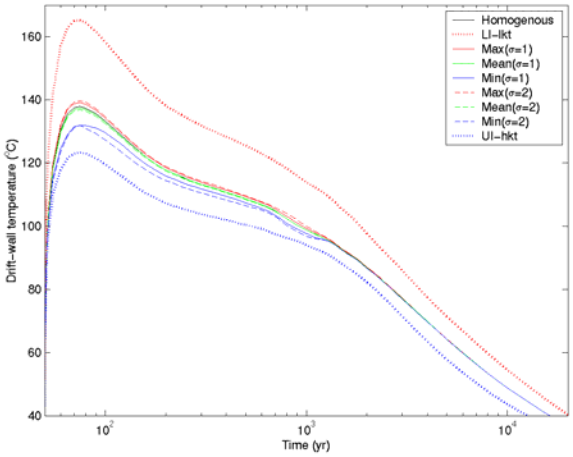

NOTE: Drift-wall temperatures are calculated by the LDTH submodel for a location close to the repository center (open circle in Fig. 4 of Buscheck et al., [10]). The drift-wall temperature is averaged around the perimeter of the drift. The ranges in drift-wall temperature for the 100 realization for $\sigma = 1.0$ and 100 realizations for $\sigma = 2.0$ are depicted by the maximum, mean, and minimum temperatures for the respective families of realizations. The range resulting from parametric uncertainty is given by the temperatures for the lower-bound-infiltration-flux/low-host-rock-thermal-conductivity (LI-lkt) and upper-bound-infiltration-flux/high-host-rock-thermal-conductivity (UI-hkt) cases.

Fig. 4. The range in drift-wall temperature for $\sigma = 1.0$ and 2.0 is compared to the homogeneous case and to the range resulting from parametric uncertainty.

TABLE II. Summary of peak drift-wall temperature

	Peak Drift-Wall Temperature (°C)				
	Heterogeneous Cases		Homogeneous Cases		
	$\sigma = 1.0$	$\sigma = 2.0$	UI-hkt[a]	MI-mkt[b]	LI-lkt[c]
Minimum	139.6	140.0	130.5	146.1	175.0
Mean	145.9	145.5			
Maximum	147.4	148.0			

NOTE: [a]UI-hkt stands for upper-bound-infiltration-flux/high-host-rock-thermal-conductivity case.

[b]MI-mkt stands for mean-infiltration-flux/mean-host-rock-thermal-conductivity case.

[c]LI-lkt stands for lower-bound-infiltration-flux/low-host-rock-thermal-conductivity case.

Fig. 6 shows the sensitivity of temperature to fracture permeability heterogeneity, using the complementary cumulative distribution function (CCDF) of peak drift-wall temperature. For 100 realizations with $\sigma = 1.0$ and 100 realizations with $\sigma = 2.0$, the peak temperature range is compared with that arising from parametric uncertainty of infiltration flux and host-rock thermal conductivity K_{th}. Peak temperature ranges for $\sigma = 1.0$ and 2.0 are insignificant compared with the range from parametric uncertainty of infiltration flux and host-rock K_{th}.

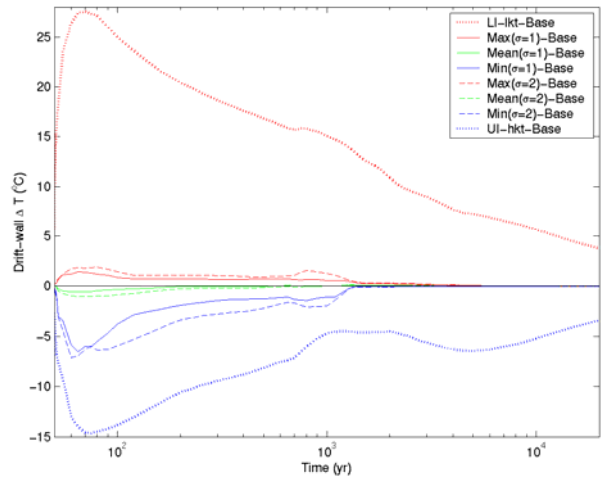

NOTE: The drift-wall "delta" temperature ΔT is the difference between the drift-wall temperature for a given heterogeneous case and that of the homogeneous (MI-mkt) case (i.e., the "Base" case). The values of ΔT pertain to Fig. 4. The range in ΔT for 100 realization for $\sigma = 1.0$ and 100 realizations for $\sigma = 2.0$ is depicted by the maximum, mean, and minimum values of ΔT for the respective families of realizations. The range in ΔT resulting from parametric uncertainty is given by the values of ΔT for the lower-bound-infiltration-flux/low-host-rock-thermal-conductivity (LI-lkt) and upper-bound-infiltration-flux/high-host-rock-thermal-conductivity (UI-hkt) cases.

Fig. 5. The range in drift-wall "delta" temperature for $\sigma = 1.0$ and 2.0 is compared to the homogeneous "base" case and to the range resulting from parametric uncertainty.

Fig. 7 uses CCDFs to show the sensitivity of the duration of boiling on the drift wall to small-scale heterogeneity in fracture permeability. For 100 realizations with $\sigma = 1.0$ and 100 realizations with $\sigma = 2.0$, the mean duration of boiling on the drift wall is nearly the same as it is for the corresponding homogeneous case. This shows that 100 realizations are sufficient to be statistically meaningful and are sufficient to capture the influence of small-scale fracture-permeability heterogeneity on flow focusing The minimum duration of boiling on the drift wall is slightly less for $\sigma = 2.0$ than it is for $\sigma = 1.0$, while the maximum duration of boiling is slightly greater for $\sigma = 2.0$ than it is for $\sigma = 1.0$. Averaged for the entire drift wall, the range in duration of boiling is 103.8 and 158.1 yr for the $\sigma = 1.0$ and 2.0, respectively, while the range in duration of boiling arising from parametric uncertainty is 1294.9 yr (Table III). Thus, the influence of small-scale fracture-permeability heterogeneity on boiling duration is insignificant compared to that of parametric uncertainty. Note that for the homogeneous case, drift-wall-averaged temperature is above 100°C for 921.6 yr, which is much less than the minimum duration of boiling (above 96°C) for all 200 heterogeneous realizations.

TABLE III. Summary of the duration of boiling on drift wall

		Duration of Boiling (T>96 °C) on the Drift Wall (yr)				
		Heterogeneous Cases		Homogeneous Cases		
		$\sigma = 1.0$	$\sigma = 2.0$	UI-hkt[a]	MI-mkt[b]	LI-lkt[c]
Averaged for Entire Drift Wall	Minimum	1173.4	1130.9	822.0	1236.4	2116.9
	Mean	1240.8	1244.8			
	Maximum	1277.2	1289.0			
Minimum for Drift Wall above Drip Shield[d]	Minimum	1230.7	1178.0	871.7	1284.3	2140.0
	Mean	1269.2	1271.9			
	Maximum	1313.9	1330.8			
Minimum for Drift Wall above Spring Line[e]	Minimum	1189.4	1148.9	871.7	1284.3	2140.0
	Mean	1261.9	1262.0			
	Maximum	1309.3	1322.3			

NOTE: [a]UI-hkt stands for upper-bound-infiltration-flux/high-host-rock-thermal-conductivity case.

[b]MI-mkt stands mean-infiltration-flux/mean-host-rock-thermal-conductivity case. The drift-wall-averaged temperature for this homogeneous case is above 100°C for 921.6 yr, which is much less than the minimum duration of boiling (96°C) for any of the 200 heterogeneous realizations.

[c]LI-lkt stands for lower-bound-infiltration-flux/low-host-rock-thermal-conductivity case.

[d]Minimum duration of boiling for the drift segment overlying the drip shield.

[e]Minimum duration of boiling for the drift segment above the spring line.

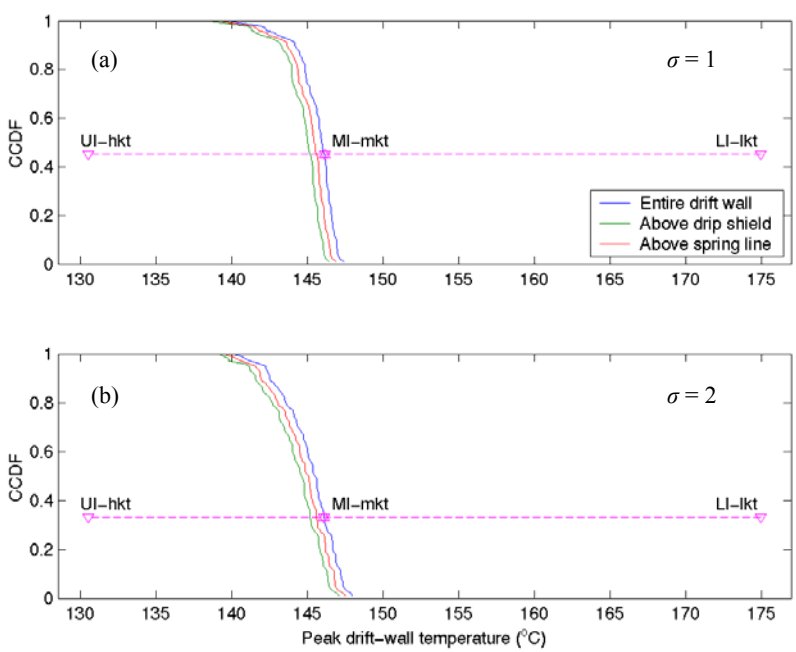

NOTE: The CCDF of peak drift-wall temperature is determined differently for the three listed drift-wall segments. For the entire drift wall, it is based on the perimeter-averaged temperature. For the segments of the drift wall above the drip shield and spring line, it is the minimum peak temperature for the given segment. The range in peak drift-wall temperatures resulting from parametric uncertainty, which is based on the perimeter-averaged temperature for the entire drift wall, is determined by the values for the lower-bound-infiltration-flux/low-host-rock-thermal-conductivity (LI-lkt) case and for the upper-bound-infiltration-flux/hight-host-rock-thermal-conductivity (UI-hkt) case. The vertical position of the magenta dashed line is determined by the intersection of the peak drift-wall-averaged temperature for the homogeneous mean-infiltration-flux/mean-host-rock-thermal-conductivity (MI-mkt) case and the CCDF curve for the entire drift wall.

Fig. 6. Complementary cumulative distribution function (CCDF) of peak drift-wall temperature for (a) 100 realizations with $\sigma = 1.0$ and for (b) 100 realizations with $\sigma = 2.0$ is compared with the range from parametric uncertainty.

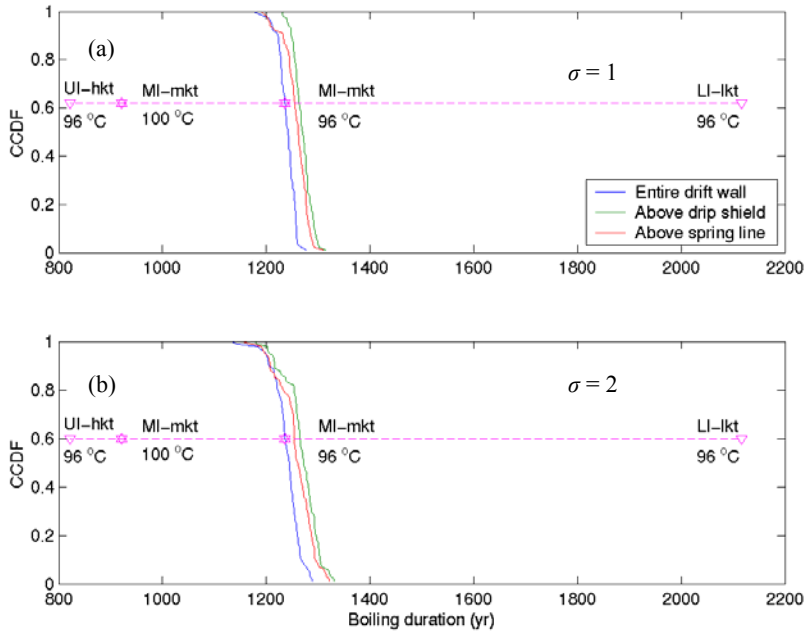

NOTE: The CCDF of drift-wall boiling duration is given for the perimeter-averaged temperature for the entire drift wall. Also given is the minimum boiling duration for the portion of the drift wall above the drip shield, and above the spring line. The minimum boiling duration is the earliest time that a location along a given drift-wall interval (e.g., above the drip shield) declines to a temperature of 96°C. The range in minimum boiling duration resulting from parametric uncertainty is given by the values for the lower-bound-infiltration-flux/low-host-rock-thermal-conductivity (LI-lkt) case and for the upper-bound-infiltration-flux/hight-host-rock-thermal-conductivity (UI-hkt) case. The vertical position of the magenta dashed line is determined by the intersection of the drift-wall-averaged boiling duration for the homogeneous mean-infiltration-flux/mean-host-rock-thermal-conductivity (MI-mkt) case and the CCDF curve for minimum boiling duration for the entire drift wall.

Fig. 7. Complementary cumulative distribution function (CCDF) of drift-wall boiling duration for (a) 100 realizations with $\sigma = 1.0$ and for (b) 100 realizations with $\sigma = 2.0$ is compared with the range resulting from parametric uncertainty.

Heating of the host rock above the boiling point of water causes boiling, vapor transport, and condensation. This causes a region of rock dryout (i.e., liquid-phase saturation less than ambient) around the drifts [9, 10], which is surrounded by the condensation zone. Those earlier studies found that the lateral extent of boiling ranges from 4.1 to 27.9 m, with a median value of 7.9 m. Note that the boiling zone and dryout zone have approximately the same lateral extent. Therefore, the maximum lateral extent of the dryout zone is much less than the 81-m spacing between drift centerlines, allowing heat-generated condensation to shed around the dryout zone and drain below the repository horizon.

The analyses of rock dryout and condensate drainage discussed above [9, 10] assumed homogeneous hydrologic properties in the host rock. An important question addressed by this study is whether small-scale fracture-permeability heterogeneity can prevent the shedding of condensate in the pillar separating emplacement drifts. To address this question, we use the quantity called the *flux ratio*. The flux ratio is equal to the total liquid-phase flux below the zone of thermal-hydrologic (TH) effects divided by the ambient percolation flux. At a distance of 40 m above the drift centerline, the influence of TH effects is negligible, such that the liquid-phase flux at that horizon can be considered to be equivalent to the ambient percolation flux. A distance of 40 m below the drift centerline is far enough removed from the dryout and condensation zones that it is completely below the zone of TH effects. Consequently, the total flux at that horizon is the result of ambient percolation flux plus heat-driven condensate flux. Therefore, we can define flux ratio to be the liquid-phase flux 40 m below the drift centerline divided by the liquid-phase flux 40 m above the drift centerline.

Fig. 8 plots the flux ratio for the 100 realizations with $\sigma = 1.0$ and the 100 realizations with $\sigma = 2.0$, as well as the flux ratio for the corresponding homogeneous case. An important observation is that the mean flux-ratio histories for both $\sigma = 1.0$ and 2.0 are essentially the same as that of the homogeneous case. Therefore, 100 realizations are sufficient to be statistically meaningful and are sufficient to capture the influence of small-scale fracture-permeability heterogeneity on condensate drainage.

Boiling causes water vapor to be driven away from the dryout region to where cooler temperatures cause it to condense. The extent to which the flux ratio exceeds 1.0 is the contribution of the condensate flux. It is also indicative of the rate at which water is being removed from the dryout zone. Thus, values of flux ratio greater than 1.0 correspond to the dryout period, when the net dryout volume is increasing. The maximum flux ratio is ~2.8 for $\sigma = 2.0$, which is slightly higher than the maximum flux ratio (~2.7) for $\sigma = 1.0$. The minimum flux ratio (~2.2) is slightly lower for $\sigma = 2.0$ than it is (~2.3) for $\sigma = 1.0$. Therefore, this range in flux ratio indicates that the volume of the dryout zone varies by about 27 percent.

Fig. 8 shows that the flux ratio abruptly increases after the preclosure ventilation period and rapidly declines to a value of 1.0 within 200 to 300 years, which corresponds to the end of the dryout period. Values of flux ratio less than 1.0 correspond to the rewetting period. During the rewetting period, which lasts for 2000 to nearly 5000 years, some of the ambient percolation flux is diverted to rewetting (by capillary imbibition) the dryout zone, which reduces the total liquid-phase flux 40 m below the drift centerline. The extent to which the flux ratio is less than zero is indicative of the rate at which water is returning to the dryout zone. The fact that the flux ratio eventually returns to a value of 1.0 indicates that 100 percent of the ambient percolation flux is able to shed through the pillar separating emplacement drifts. Therefore, small-scale fracture-permeability heterogeneity does not prevent the shedding of condensate in the pillar separating emplacement drifts.

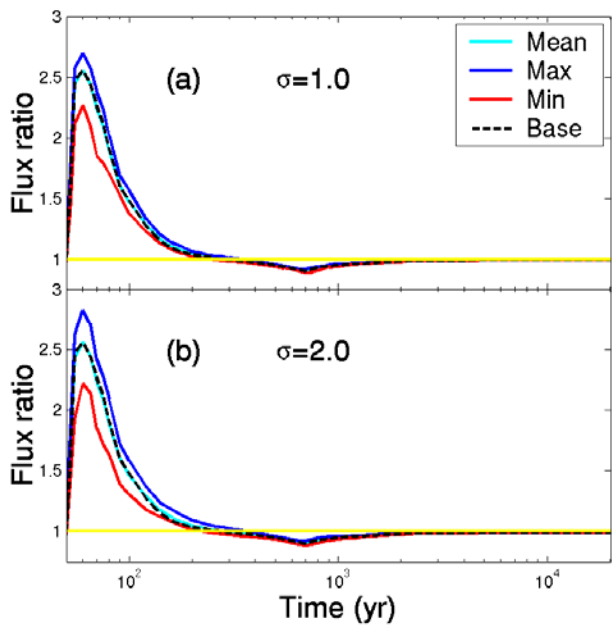

NOTE: The flux ratio is the total vertical liquid-phase flux crossing the plane 40 m below the drift centerline divided by the total liquid-phase flux crossing the plane 40 m above the drift centerline. The liquid-phase flux 40 m above the drift centerline is equivalent to the ambient percolation flux. The liquid-phase flux 40 m below the drift centerline is equivalent to the thermally-altered liquid-phase flux. The maximum (max), mean, and minimum (min) flux ratios are for the each of the respective families of 100 realizations. The "base" case flux ratio is applicable to the homogeneous case.

Fig. 8. The flux ratio is plotted for (a) 100 realizations with $\sigma = 1.0$ and for (b) 100 realizations with $\sigma = 2.0$ and is compared with the flux ratio for the homogeneous case.

IV. CONCLUSIONS AND DISCUSSION

A sensitivity study is conducted to investigate the influence of small-scale heterogeneity in fracture permeability on near-field and in-drift thermal-hydrologic (TH) behavior, with an emphasis on temperature. For a location close to the center of the Yucca Mountain repository, an LDTH submodel from the Multiscale Thermohydrologic Model (MSTHM) is applied to conduct 20,100-yr calculations for two groups of 100 realizations each. Over the entire interval between the drift and pillar centerlines, the minimum focus factor is close to zero and the maximum focus factor has little variability for each group of 100 realizations. Moreover, the mean temperature history for each group of 100 realizations is close to the temperature history for the corresponding homogeneous case. Therefore, 100 realizations are statistically meaningful and are thereby sufficient to capture the influence of small-scale fracture-permeability heterogeneity on flow focusing.

The influence of small-scale heterogeneity in fracture permeability, and the resulting small-scale flow focusing, has an insignificant effect of the temperature history compared to the influence of parametric uncertainty that has been addressed by the MSTHM. Therefore, it is not necessary to propagate the influence of small-scale fracture-permeability heterogeneity through the MSTHM predictions supporting the performance assessment of the proposed nuclear-waste repository at Yucca Mountain.

An examination of rock dryout and condensate drainage indicates that small-scale heterogeneity in fracture permeability results in a relatively small range in dryout volume. That analysis also shows that small-scale heterogeneity in fracture permeability does not prevent the shedding of condensate through the pillar separating emplacement drifts.

ACKNOWLEDGMENTS

We gratefully acknowledge the review of Tom Wolery. This work was performed under the auspices of the U.S. Department of Energy by University of California Lawrence Livermore National Laboratory under contract No. W-7405-Eng-48.

REFERENCES

1. L.W. GELHAR, *Stochastic Subsurface Hydrology*, Prentice-Hall, Englewood Cliffs, NJ, 1993.
2. A.F.B. TOMPSON, K.J. JACKSON, "Reactive transport in heterogeneous systems", *Rev. Miner.* **34**, 1, 269–308 (1996).
3. Q. ZHOU, H.H. LIU, G.S. BODVARSSON, C.M. OLDENBURG, "Flow and transport in unsaturated fractured rock: effects of multiscale heterogeneity of hydrogeologic properties,**"** *J. Contam. Hydrol.* **60**, 1–30 (2003).
4. S.A. MCKENNA, D.D. WALKER, B. ARNOLD, "Modeling dispersion in three-dimensional heterogeneous fractured media at Yucca Mountain," *J. Contam. Hydrol.*, **62–63**, 577–594 (2003).
5. H.S. VISWANATHAN, B.A. ROBINSON, C.W. GABLE, J.W. CAREY, "A geostatistical modeling study of the effect of heterogeneity on radionuclide transport in the unsaturated zone, Yucca Mountain," *J. Contam. Hydrol.* **62–63**, 319–336 (2003).
6. BSC (BECHTEL SAIC), Seepage calibration model and seepage testing data, MDL-NBS-HS-000004, REV 3, Las Vegas, NV (2004).
7. BSC (BECHTEL SAIC), Abstraction of drift seepage, MDL-NBS-HS-000019, REV 1, Las Vegas, NV (2004).
8. BSC (BECHTEL SAIC), Drift-scale coupled processes (DST and TH seepage) models, MDL-NBS-HS-000015, REV 2, Las Vegas, NV (2005).
9. BSC (BECHTEL SAIC), Multiscale Thermohydrologic Model, ANL-EBS-MD-000049 REV 3, Las Vegas, NV (2005).
10. T.A. BUSCHECK, Y. SUN, AND Y. HAO, "Multiscale Thermohydrologic Model supporting the License Application for the Yucca Mountain Repository," *Proc. of International High-Level Radioactive Waste Management Conference*, Las Vegas, NV, April 30 – May 4, American Nuclear Society, LaGrange Park, IL (2006).
11. L.G. GLASCOE, T.A. BUSCHECK, J. GANSEMER, Y. SUN, K. LEE, Multiscale thermohydrologic model analyses of heterogeneity and thermal-loading factors for a proposed nuclear waste repository, *Nucl. Technol.* **148**, 2, 125—137 (2004).
12. T.A. BUSCHECK, N.D. ROSENBERG, J. GANSEMER, Y. SUN, "Thermohydrologic behavior at an underground nuclear waste repository,*" Water Resour. Res.* **38**, 3, 10.1029 (2002).
13. M.T.A. VAN GENUCHTEN, "A closed-form equation for predicting the hydraulic conductivity of unsaturated soils," *Soil Sci. Sci. Am. J.*, **44**, 892–898 (1980).
14. H.H. LIU, C. DOUGHTY, G.S. BODVARSSON, "An active fracture model for unsaturated flow and transport in fractured rock," *Water Resour. Res.* **34**, 10, 2633–2646 (1998).